*J. Fluid Mech.* (1997), *vol.* 339, *pp.* 331–356. Printed in the United Kingdom



# Trapped modes about multiple cylinders in a channel

By D. V. EVANS AND R. PORTER

School of Mathematics, University of Bristol, Bristol, BS8 1TW, UK

(Received 23 September 1996 and in revised form 20 December 1996)

The trapped modes which can occur in a long narrow wave channel containing any number of different-sized bottom-mounted circular cylinders arbitrarily spaced along the centreline of the channel are considered. The modes, all of which are antisymmetric with respect to the centreplane of the channel are of two types: Neumann modes, in which the fluid has normal velocity zero on the channel walls corresponding to a localized sloshing near the cylinders, and Dirichlet modes, in which the dynamic pressure vanishes on the channel walls. These latter modes have no physical meaning in the water-wave context but have been observed in a related acoustic context where the same governing equations and boundary conditions apply.

It is shown that in general there are $\leqslant N$ trapped modes for any configuration of $N$ cylinders, the precise number depending critically on the geometry of the configuration. Both types are of importance in predicting the exciting forces on individual cylinders within a large but finite periodic arrangement of cylinders.

## 1. Introduction

The existence of trapped modes in the presence of a single rigid vertical circular cylinder placed on the centreline and extending throughout the depth of a long narrow wave channel was first demonstrated by Callan, Linton & Evans (1991) for sufficiently small cylinders. The governing equations also describe the trapped modes near a symmetrically placed rigid circular boundary in a two-dimensional acoustic waveguide. Numerical computations made by Callan *et al.* (1991) indicated that just a single trapped mode existed for each value of $a/d \leqslant 1$ where $a$ is the cylinder radius and $2d$ is the width of the channel. Recent careful experiments by C. H. Retzler (private communication, 1996) have confirmed the predicted trapped mode frequencies of Callan *et al.* (1991) for three different-sized circular cylinders. The trapped modes take the form of a persistent local oscillation near the cylinder at a unique frequency below the first cut-off frequency for the channel, and are antisymmetric with respect to the centreplane of the channel and symmetric with respect to a plane through the axis of the cylinder perpendicular to the sides of the channel.

A numerical method using an appropriate Green function for determining trapped modes for more general cylinders in terms of homogeneous solutions of a Fredholm integral equation was presented in Linton & Evans (1992). In particular the results give good agreement with Callan *et al.* (1991) in the circular cylinder case. Subsequently Evans, Levitin & Vassiliev (1994) proved the existence of trapped modes for a general class of cylinders placed symmetrically with respect to the channel centreplane and

on which a Dirichlet condition is satisfied by the potential function describing the motion thereby ensuring that the motion was antisymmetric with respect to this plane. More recently this work has been extended by Davies & Parnovski (1997) to include, for example, a pair of identical cylinders being reflections of each other in the centreplane. They provide both existence and non-existence results for trapped modes depending on the shape, size and position of the obstacle(s) in the channel or acoustic waveguide.

In this paper we return to the case of the circular cylinder on the centreplane and generalize the results of Callan *et al.* (1991) to the case of any number of circular cylinders of arbitrary size, all positioned on the centreplane. The motivation for this is three-fold. First, current theory says nothing about the number of trapped waves in the case of separate cylinders placed along the centreplane. Secondly, some interesting questions arise. For instance, since trapped modes are a localized phenomenon, one might expect that for $N$ ($> 1$) different-sized circular cylinders spaced sufficiently far apart there will be $N$ distinct trapped mode frequency curves each approaching its respective value for the corresponding single cylinder as spacing increases. The question arises as to what happens as the spacing *decreases* until the cylinders touch. Do the $N$ curves coalesce or do some disappear at some critical spacing for certain sized cylinders ? For example, computations by Evans & Linton (1991) of the trapped modes in the case of a cylinder of rectangular cross-section indicate that additional trapped modes only arise if the dimension of the rectangle in the direction of the sides of the channel exceeds the width of the channel.

Finally, the importance of trapped modes in the offshore industry has been brought into prominence recently by the work of Maniar & Newman (1997) who have discovered extremely large wave diffraction forces and corresponding large amplitudes of free-surface elevations between adjacent elements of an array consisting of a large number of identical bottom-mounted circular cylinders. These effects occur at frequencies extremely close to the trapped mode frequencies predicted by the theory of Callan *et al.* (1991) and tabulated in Linton & Evans (1992). Maniar & Newman (1997) point out that such periodic arrays have applications to structures such as floating bridges or proposed designs for floating airports. In practice, however, it is clear that at least a double array of supporting cylinders will be needed so that it is important to predict the corresponding trapped mode frequencies for more than a single cylinder on the centreplane.

In order to illustrate how large forces can occur in even a relatively small double array of cylinders, we have computed in figure 1 the maximum total force on the middle pair of cylinders in a double array of $2 \times 9$ cylinders in head seas using the interaction theory of Linton & Evans (1990). The different curves refer to different-sized cylinders. This theory enables the exciting force on any bottom-mounted circular cylinder in an array of cylinders of arbitrary size and position to be determined by solving an infinite system of equations for unknown Fourier-type coefficients, $A_k$. The exciting forces turn out simply to involve sums and differences of $A_1$ and $A_{-1}$. It is clear from figure 1 that at well-defined wavenumbers or frequencies, the maximum total force on the cylinders in the middle of the row becomes large. Indeed, these peaks in the force are present (to a lesser extent) in the force curves for all elements in the array. We shall show that in each curve the first peak located at $\kappa d < \frac{1}{2}\pi$ approximates to the wavenumber of the symmetric trapped mode which arises in the case of two such cylinders spaced with centres two cylinder diameters apart in a wave-tank of width $2d$. The peak lying in $\frac{1}{2}\pi < \kappa d < \pi$ will be shown to approximate to the symmetric Dirichlet trapped mode described in Maniar & Newman (1997). In the water-wave

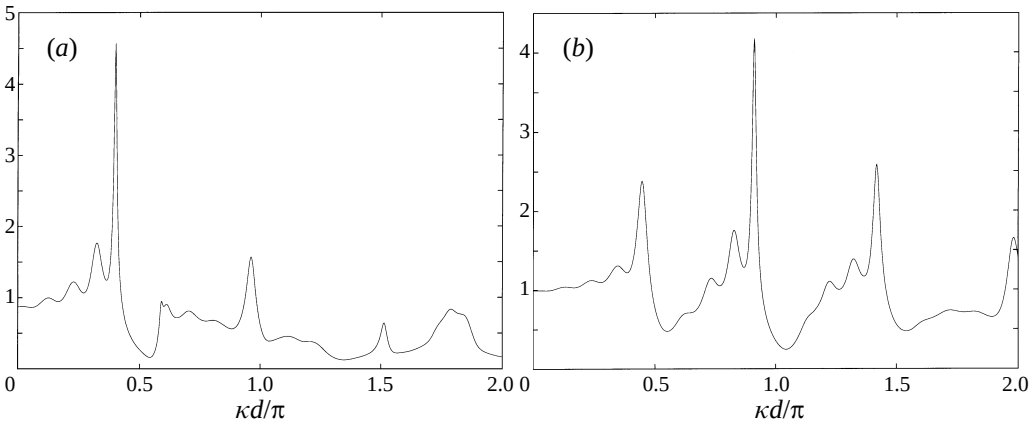


FIGURE 1. Maximum exciting force against non-dimensional wavenumber $\kappa d$ in the case of head seas interacting with a double array of $2 \times 9$ cylinders all of radius $a$. The two rows are $4a$ apart and in each row the centres are $2d$ apart. (*a*) $a/d = \frac{1}{2}$, (*b*) $a/d = \frac{1}{4}$.

context this is a non-physical trapped mode satisfying Dirichlet conditions on the tank walls as well as on the centreplane, thereby extending the cut-off to $\kappa d = \pi$, but as Maniar & Newman (1997) have pointed out, such modes are important in understanding the large forces and free-surface amplitudes of motion which occur in long finite arrays of cylinders near Dirichlet frequencies. Such Dirichlet modes are well-known in acoustics and have been observed in wind tunnels containing cascades of flat horizontal plates spanning the full width of the tunnel. For an extensive review of such acoustic resonances, see Parker & Stoneman (1989). An approximate but accurate formula for predicting the Dirichlet resonant frequencies near a thin plate is given by Evans & Linton (1994), whilst McIver & Linton (1995) have produced non-existence results for Dirichlet modes for certain geometries including the case of multiple cylinders discussed here. They relax the requirement of a Dirichlet condition on the centreplane so that the corresponding possibility of modes satisfying $\frac{1}{2}\pi < \kappa d < \pi$ does not arise.

The plan of the paper is as follows. In the next section we formulate the problem and solve the problem of determining all the trapped modes which can occur when any number of rigid bottom-mounted vertical circular cylinders are placed on the centreplane of a channel. The cylinders can have any radii and can be spaced arbitrarily and we seek trapped modes which are antisymmetric about the centreplane and satisfy Neumann conditions on the channel walls. Henceforth we call such modes Neumann modes.

The solution is based on the multipole method, in which singular solutions of the Helmholtz equation satisfying an antisymmetry condition on the channel centreplane are modified to include the boundary conditions on the channel walls. The total potential about any cylinder may then be expressed as a Fourier-type sum over all relevant multipoles and the total potential anywhere in the channel as the sum over all cylinders. The remaining condition to be satisfied, that of no-flow on the cylinder surfaces, is achieved by use of a Bessel function addition theorem, as in Linton & Evans (1990), yielding a homogeneous determinant system whose non-trivial solutions correspond to the trapped mode frequencies. The same method has recently been used by Linton & McIver (1996) to determine the scattering properties of any number of circular cylinders of arbitrary size and position in a channel. The

method is an extension of that used by Callan *et al.* (1991) for the single cylinder. Crucial to that method was the fact that the channel multipoles turned out to be purely imaginary leading to a homogeneous real infinite system of equations. It turns out that here too the more general multipoles in which symmetry about the plane through the centre of a cylinder perpendicular to the channel walls is not assumed also turn out to be pure imaginary and again produce a real system of equations.

Also in §2 a description is given of the changes necessary to treat the Dirichlet trapped modes for any number of circular cylinders. The potential now satisfies a Dirichlet condition on the channel walls and since the modifications turn out to be minor the details are omitted. Despite the similarity in derivation there is a fundamental qualitative difference in behaviour of Neumann and Dirichlet trapped modes. Thus, whereas for a single circular cylinder Callan *et al.* (1991) showed that a trapped mode exists for all $a/d \leqslant 1$, the corresponding Dirichlet trapped mode has been shown by Maniar & Newman (1997) to occur provided $a/d \lesssim 0.677$. It is easy to see how such a geometric cut-off might arise by considering the Dirichlet trapped modes which occur in the simplest case of a cylinder of rectangular cross-section on the centreplane. An examination of the possible modes which can exist in the region between the channel walls and the side of the rectangle on which Dirichlet and Neumann conditions are to be satisfied respectively, and the region between the channel walls and the centreplane on each of which a Dirichlet condition holds, shows that in order for the lowest cut-off to exist, it is necessary that $b/d < \frac{1}{2}$ where $b(d)$ is the half-width of the rectangle (channel). Both the Neumann and Dirichlet trapped modes for a rectangle have recently been computed by the authors using a powerful Galerkin method used in related scattering problems. See, for example, Porter (1995) and Evans & Fernyhough (1995) who solve the general problem of Rayleigh–Bloch waves along a periodic rectangular coastline. The computations confirm the condition $b/d < \frac{1}{2}$ for Dirichlet modes near rectangular cylinders. In §2.4 the existence or otherwise of Dirichlet modes is discussed and new results presented guaranteeing their existence in the case of single cylinders of arbitrary cross-section on the centreplane.

It should be emphasized that the success of the method depends upon obtaining a real infinite system of equations in the Neumann case with $\kappa d < \frac{1}{2}\pi$ and in the Dirichlet case with $\frac{1}{2}\pi < \kappa d < \pi$. For $\kappa d$ above these values the systems are complex and the question of the existence of trapped modes is less clear. However, recently the authors (Evans & Porter 1997) have provided strong numerical evidence that such trapped modes embedded in the continuous spectrum do indeed exist but only for a single wavenumber at a precise value of $a/d$ for both the Neumann and Dirichlet cases.

Results are presented in §3 in the form of curves describing the variation of non-dimensional trapped mode wavenumber with different parameters for a variety of cylinder configurations for both Neumann and Dirichlet modes. Because of their importance in applications special attention is paid to the case of two identical cylinders. Other cases considered include two or three different-sized cylinders and four identical equally spaced cylinders. Also shown are curves illustrating the relative amplitudes of motion of the trapped modes in one or two cases. The details of the analysis, including the derivation of the multipoles and the application of the Bessel addition theorem are relegated to Appendices.

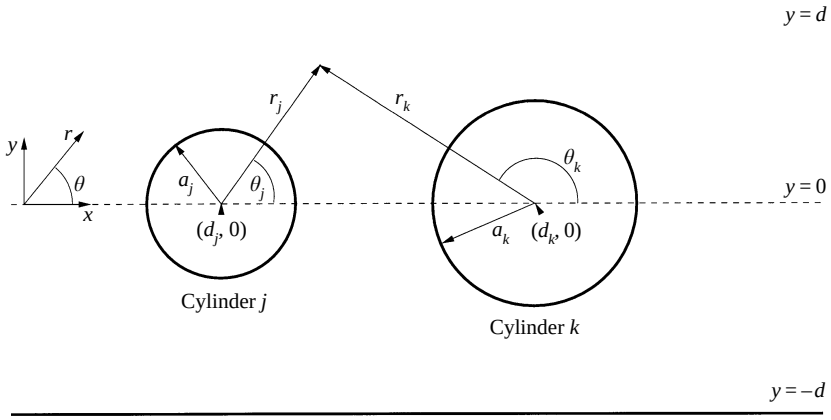


FIGURE 2. Plan view of two cylinders in a channel.

## 2. Formulation

### 2.1. *Formulation of the problem for Neumann modes*

The origin is placed in the free surface midway between parallel channel walls situated at $y = \pm d$. The $z$-axis is measured vertically upwards with the channel bottom at $z = -h$ and the undisturbed free surface at $z = 0$. Polar coordinates will also be used and are defined in the usual manner: $x = r\cos\theta$, $y = r\sin\theta$. $N$ fixed vertical circular cylinders are placed on the centreplane of the channel and extend uniformly throughout the depth. The $j$th cylinder is given a radius $a_j$ and its centre positioned at $(x, y) = (d_j, 0)$, $j = 1, 2, \ldots, N$. It is convenient to define local polar coordinates $(r_j, \theta_j)$ associated with cylinder $j$ (see figure 2).

Under the usual assumptions of linear water-wave theory, we assume a velocity potential, $\Phi(x, y, z, t)$, which is expressed as

$$\Phi(x, y, z, t) = \mathrm{Re}\left\{\phi(x, y) f(z) \mathrm{e}^{-\mathrm{i}\omega t}\right\} \tag{2.1}$$

where

$$f(z) = -\mathrm{i}gA \cosh\kappa(z + h)/\omega \cosh\kappa h \tag{2.2}$$

and where the depth dependence has been extracted and time-harmonic motion of angular frequency $\omega$ is assumed with the wavenumber $\kappa$ the positive root of the usual dispersion relation

$$\omega^2/g = \kappa \tanh\kappa h. \tag{2.3}$$

Then $\phi$ satisfies the Helmholtz equation,

$$(\nabla^2 + \kappa^2)\phi(x, y) = 0 \tag{2.4}$$

exterior to the cylinders,

$$\frac{\partial\phi}{\partial r_j} = 0 \qquad \text{on } r_j = a_j,\ j = 1, \ldots, N \tag{2.5}$$

expressing no-flow through the cylinders and on the channel walls, $y = \pm d$, the condition

$$\frac{\partial\phi}{\partial y} = 0 \qquad \text{for Neumann modes,} \tag{2.6}$$

$$\phi = 0 \qquad \text{for Dirichlet modes.} \tag{2.7}$$

For most of this section we shall restrict our attention to Neumann trapped modes satisfying (2.6); the changes necessary for Dirichlet trapped modes satisfying (2.7) will be outlined in §2.4.

In seeking a trapped mode, we also require the potential to be antisymmetric about the channel centreplane and decay away from the cylinders. Thus

$$\phi(x,0) = 0, \qquad -\infty < x < \infty \tag{2.8}$$

and

$$\phi(x,y) \to 0 \qquad \text{as } |x| \to \infty, \ -d \leqslant y \leqslant d. \tag{2.9}$$

We only consider the solution in $0 < y < d$ ($0 < \theta < \pi$) with the extension to $-d < y < 0$ given by $\phi(x,-y) = -\phi(x,y)$ as a direct consequence of condition (2.8).

Note that in the context of acoustics, rather than water waves, we would write $\Phi = \mathrm{Re}\{\phi \mathrm{e}^{-\mathrm{i}\omega t}\}$ where $\kappa = \omega/c$ and $c$ is the speed of sound.

We introduce the multipole potentials (see Appendix A) based on cylinder $j$ by

$$\psi_n^j(r_j,\theta_j) = Y_n(\kappa r_j)\sin n\theta_j - \mathrm{Re}\frac{1}{\pi}\int_{-\infty}^{\mathrm{i}\pi+\infty} \frac{\mathrm{e}^{\gamma d - nv}}{\cosh \gamma d}\sinh \gamma y_j \sin(\kappa x_j \cosh v - n\pi/2)\,\mathrm{d}v \tag{2.10}$$

where $\gamma = \kappa \sinh v$, using local coordinates $x_j = r_j\cos\theta_j$, $y_j = r_j \sin\theta_j$ about the centre, $(d_j, 0)$, of cylinder $j$. They satisfy

$$\begin{aligned} (\nabla^2 + \kappa^2)\psi_n^j &= 0, \qquad r_j \neq 0 \\ \psi_n^j(r_j,0) = \psi_n^j(r_j,\pi) &= 0, \\ \frac{\partial \psi_n^j}{\partial y} &= 0 \qquad \text{on } y = d \\ \psi_n^j &\to 0 \qquad \text{as } |x| \to \infty \text{ for } \kappa < \pi/2d. \end{aligned}$$

We then construct possible trapped mode potentials as the sum over all multipoles and all cylinders:

$$\phi(r,\theta) = \sum_{j=1}^{N}\sum_{n=1}^{\infty} A_n^j \psi_n^j(r_j,\theta_j) \tag{2.11}$$

for some constants, $A_n^j$, by looking for possible non-trivial solutions satisfying the remaining condition on the cylinders, namely (2.5). In order to impose this condition, we need to shift from the local coordinates of a typical cylinder $j$ to a cylinder $k$, say. Thus, from Appendix B, we have the result

$$Y_n(\kappa r_j)\sin n\theta_j = \sum_{m=1}^{\infty} F_{mn}^{jk} J_m(\kappa r_k)\sin m\theta_k, \tag{2.12}$$

with $F_{mn}^{jk}$ defined by (B2) and from (B8) we have

$$\begin{aligned} &\sinh \gamma y_j \sin(\kappa x \cosh y_j - n\pi/2) \\ &\quad = -2\sum_{m=1}^{\infty} \cos\{\kappa(d_k - d_j)\cosh v + \tfrac{1}{2}(m-n)\pi\} J_m(\kappa r_k)\sin m\theta_k \sinh mv. \end{aligned} \tag{2.13}$$

It follows from (2.10), (2.12), (2.13), that

$$\psi_n^j(r_j,\theta_j) = Y_n(\kappa r_j)\sin n\theta_j + \sum_{m=1}^{\infty} C_{mn}J_m(\kappa a_j)\sin m\theta_j,$$

$$= \sum_{m=1}^{\infty}\left(F_{mn}^{jk} + C_{mn}^{jk}\right)J_m(\kappa r_k)\sin m\theta_k, \qquad j \neq k \tag{2.14}$$

where

$$C_{mn}^{jk} = \mathrm{Re}\frac{2}{\pi}\int_{-\infty}^{\mathrm{i}\pi+\infty} \frac{\mathrm{e}^{\gamma d - nv}\sinh mv}{\cosh \gamma d}\cos\{\kappa(d_k - d_j)\cosh v + \tfrac{1}{2}(m-n)\pi\}\,\mathrm{d}v. \tag{2.15}$$

Note that $C_{mn}^{jk} = (-1)^{m-n}C_{mn}^{kj}$. We have also written

$$C_{mn}^{kk} \equiv C_{mn} = \mathrm{Re}\frac{2}{\pi}\int_{-\infty}^{\mathrm{i}\pi+\infty} \frac{\mathrm{e}^{\gamma d - nv}\sinh mv}{\cosh \gamma d}\cos \tfrac{1}{2}(m-n)\pi\,\mathrm{d}v. \tag{2.16}$$

We now may write

$$\phi(r,\theta) = \sum_{n=1}^{\infty} A_n^k \psi_n^k(r_k,\theta_k) + \sum_{\substack{j=1\\ \neq k}}^{N}\sum_{n=1}^{\infty} A_n^j \psi_n^j(r_j,\theta_j) \tag{2.17}$$

and so imposing (2.5) by using (2.14) gives

$$0 = \frac{1}{\kappa}\frac{\partial\phi}{\partial r_k}\bigg|_{r_k=a_k} = \sum_{n=1}^{\infty} A_n^k\left\{Y_n'(\kappa a_k)\sin n\theta_k + \sum_{m=1}^{\infty} C_{mn}J_m'(\kappa a_k)\sin m\theta_k\right\}$$

$$+ \sum_{\substack{j=1\\ \neq k}}^{N}\sum_{n=1}^{\infty} A_n^j \sum_{m=1}^{\infty}\left(F_{mn}^{jk} + C_{mn}^{jk}\right)J_m'(\kappa a_k)\sin m\theta_k, \quad k = 1,\ldots,N. \tag{2.18}$$

Equating coefficients of $\sin m\theta_k$:

$$A_m^k Y_m'(\kappa a_k) + J_m'(\kappa a_k)\sum_{n=1}^{\infty} A_n^k C_{mn} + J_m'(\kappa a_k)\sum_{\substack{j=1\\ \neq k}}^{N}\sum_{n=1}^{\infty} A_n^j\left(F_{mn}^{jk} + C_{mn}^{jk}\right) = 0,$$

$$k = 1,\ldots,N;\ m = 1,2,\ldots \tag{2.19}$$

This is the system whose non-trivial solutions determine the trapped mode frequencies. It is also possible to derive a simple expression for the potential in the vicinity of cylinder $k$ using the same technique as, for example, Linton & Evans (1990) of substituting the infinite system of equations (2.19) back into the expression for the potential $\phi(r_k,\theta_k)$ about the $k$th cylinder. This results in

$$\phi(r_k,\theta_k) = \sum_{m=1}^{\infty} A_m^k \sin m\theta_k\left\{Y_m(\kappa r_k) - \frac{Y_m'(\kappa a_k)}{J_m'(\kappa a_k)}J_m(\kappa r_k)\right\} \tag{2.20}$$

which is valid within the limitations of Graf's Addition Theorem, that is for $r_k < |d_k - d_j|$, $\forall j \neq k$.

### 2.2. *Two equal cylinders*

In the case of two identical cylinders ($a_1 = a_2 = a$) placed at $d_1 = -d_2$ we may exploit the geometric symmetry and look for a potential exhibiting a trapped mode

that is either odd or even about the plane $x = 0$. This allows the system (2.19) to be simplified in the following manner.

An even/odd solution implies $\phi(x, y) = \pm\phi(-x, y)$ respectively. From (2.11) this requires

$$0 = \sum_{n=1}^{\infty} \left\{ A_n^1 \psi_n^1(r_1, \theta_1) \mp A_n^2 \psi_n^2(r_1, \pi - \theta_1) \right\}. \tag{2.21}$$

But from (2.14)

$$\begin{aligned} \psi_n^2(r_1, \pi - \theta_1) &= Y_n(\kappa r_1)(-1)^{n+1} \sin n\theta_1 + \sum_{m=1}^{\infty} C_{mn} J_m(\kappa r_1)(-1)^{m+1} \sin m\theta_1 \\ &= (-1)^{n+1} \psi_n^1(r_1, \theta_1) \end{aligned} \tag{2.22}$$

once we have used $(-1)^{m-n} C_{mn} = C_{mn}$ since $C_{mn} = 0$ for $m - n$ odd. Thus from (2.21),

$$A_n^1 = \pm(-1)^{n+1} A_n^2 \qquad \text{for even/odd solutions resp.} \tag{2.23}$$

Using this in the original coupled system, (2.19), reduces it simply to

$$A_m^1 Y_m'(\kappa a) + J_m'(\kappa a) \sum_{n=1}^{\infty} A_n^1 \left\{ C_{mn} + (-1)^{n+s} (F_{mn}^{21} + C_{mn}^{21}) \right\} = 0, \tag{2.24}$$

where $s = 1$ (0) denotes an even (odd) solution. This process could clearly be repeated for symmetrical arrangements involving larger numbers of cylinders.

### 2.3. *Computations*

In order to compute the determinant of (2.19) we need $F_{mn}^{jk}$, given in Appendix B, and we need to evaluate the integrals in (2.15) and (2.16) to determine $C_{mn}$ and $C_{mn}^{jk}$. This is done by dividing the contour integral into the three parts described in Appendix A, namely $C_1 = (-\infty, 0)$, $C_2 = (0, \mathrm{i}\pi)$, $C_3 = (\mathrm{i}\pi, \mathrm{i}\pi + \infty)$ and using variable changes $v = -u$, $v = \mathrm{i}(u + \frac{1}{2}\pi)$, $v = \mathrm{i}\pi + u$ respectively to give

$$C_{mn}^{jk} = D_{mn}^{jk} + E_{mn}^{jk}, \tag{2.25}$$

where

$$D_{mn}^{jk} = -\frac{4}{\pi} \int_0^{\infty} \frac{\mathrm{e}^{-\gamma d}}{\cosh \gamma d} \sinh mv \sinh nv \cos\{\kappa(d_k - d_j) \cosh v + \tfrac{1}{2}(m - n)\pi\} \, \mathrm{d}v \tag{2.26}$$

whilst we consider all even/odd combinations of $n$, $m$ for $E_{mn}^{jk}$ (from the line segment $C_2$):

$$E_{2p,2q}^{jk} = -\frac{4}{\pi} \int_0^{\pi/2} \tan(\beta d) \sin 2pu \sin 2qu \cos\{\kappa(d_k - d_j) \sin u\} \, \mathrm{d}u, \tag{2.27}$$

$$E_{2p+1,2q+1}^{jk} = -\frac{4}{\pi} \int_0^{\pi/2} \tan(\beta d) \cos(2p+1)u \cos(2q+1)u \cos\{\kappa(d_k - d_j) \sin u\} \, \mathrm{d}u, \tag{2.28}$$

$$E_{2p+1,2q}^{jk} = -\frac{4}{\pi} \int_0^{\pi/2} \tan(\beta d) \cos(2p+1)u \sin 2qu \sin\{\kappa(d_k - d_j) \sin u\} \, \mathrm{d}u, \tag{2.29}$$

$$E_{2p,2q+1}^{jk} = +\frac{4}{\pi} \int_0^{\pi/2} \tan(\beta d) \sin 2pu \cos(2q+1)u \sin\{\kappa(d_k - d_j) \sin u\} \, \mathrm{d}u. \tag{2.30}$$

Note that $C_{mn} = C^{kk}_{mn}$, and in this case $d_k - d_j = 0$ simplifies the above expressions through the cos and sin factors.

It is clear from the equations above that $C^{jk}_{mn} = (-1)^{m-n} C^{jk}_{nm}$, providing yet another symmetry relation that can be exploited to enhance computational efficiency.

### 2.4. *Dirichlet trapped modes*

Dirichlet trapped modes require (2.7) to be satisfied instead of the Neumann channel wall condition, (2.6). The potential in this non-physical channel is now a sum over multipoles which differ from those used in §§2.1–2.3 by the fact that they satisfy Dirichlet conditions on $y = \pm d$. In fact, these Dirichlet multipoles are shown in Appendix A to be very similar to those in the Neumann case, the only change being the replacement of $\cosh \gamma d$ by $\sinh \gamma d$ in the denominator of the integrand. The resulting changes in the analysis of §§2.1–2.3 are therefore confined solely to those parts which rely on the form of the multipoles. Thus the systems to be solved for the general cylinder configuration and the two equal-cylinder case are still (2.19) and (2.23) respectively, but with different $C_{mn}$, $C^{jk}_{mn}$. These coefficients are determined in the same fashion as in the Neumann case and it turns out that the only changes requires in the computations of $C_{mn}$, $C^{jk}_{mn}$ are that $\cosh \gamma d$ is replaced by $-\sinh \gamma d$ in (2.26) and $\tan \beta d$ is replaced by $-\cot \beta d$ in (2.27)–(2.30).

The case of a single cylinder can also be determined from the general formulation. Thus in (2.19) the last term is omitted and using the fact that $C_{mn} = 0$ for $m - n$ odd the system decouples leaving

$$A^1_{2m} Y'_{2m}(\kappa a_1) + J'_{2m}(\kappa a_1) \sum_{n=1}^{\infty} A^1_{2n} C_{2m,2n} = 0 \tag{2.31}$$

and

$$A^1_{2m+1} Y'_{2m+1}(\kappa a_1) + J'_{2m+1}(\kappa a_1) \sum_{n=1}^{\infty} A^1_{2n+1} C_{2m+1,2n+1} = 0 \tag{2.32}$$

corresponding to odd and even potentials about the plane of symmetry through the centre of the cylinder and perpendicular to the channel walls respectively. It turns out that (2.31) has no solution and so the Dirichlet trapped modes for a single cylinder are determined by the system (2.32) with the appropriate modifications to $C_{2m+1,2n+1}$ in (2.25) outlined above.

It is of interest to derive this result directly using the methods of Callan *et al.* (1991). Thus referring to that paper, the modifications required are the substitution of $\cosh \gamma d$ and $\tan \beta d$ in their equation (2.10) with $-\sinh \gamma d$ and $-\cot \beta d$ for use in their system (2.13) in agreement with the reduced form of the general system, (2.32), above.

As mentioned in the Introduction, we expect to find fundamental differences in the conditions for existence of Dirichlet and Neumann trapped modes. Evans *et al.* (1994) have shown that for a cylinder of fairly general cross-section, positioned on and symmetric about the centreplane, there always exists a Neumann trapped mode. If however one considers disjoint cylinders being reflections of each other in the centreplane, the situation is much more complicated. Thus Davies & Parnovski (1996) have shown that the existence or otherwise of Neumann modes is highly sensitive to geometry whilst for the same geometry of disjoint cylinders McIver & Linton (1995) have provided a simple geometric condition under which Dirichlet trapped modes satisfying $\kappa d < \frac{1}{2}\pi$ do not exist. For a single cylinder of fairly arbitrary cross-section on the centreplane it proves possible to extend the methods

of Evans *et al.* (1994) to cover the Dirichlet case. Thus if the cross-section of the cylinder is described by $y = f(x)$, $f(\pm a) = 0$, $0 \leqslant f(x) < d$, $|x| \leqslant a$, it can be shown that Dirichlet modes exist provided

$$I = \int_{-a}^{a} \sin(2\pi f(x)/d)\, \mathrm{d}x > 0. \tag{2.33}$$

For example, for a rectangular block with $f(x) = b$, $|x| \leqslant a$, this gives $b/d < \frac{1}{2}$ as expected and it is immediately clear from (2.33) that provided $f(x) < d/2$, $I > 0$ and so a trapped mode exists for all $f$. The circular cylinder gives $I = \pi a J_1(2\pi a/d) > 0$ provided $a/d \lesssim 0.6098$ consistent with the figure 0.677 computed by Maniar & Newman (1997). By considering cylinders having cross-sections described by $(x/a)^n + (y/b)^n = 1$ for different $n > 0$ it is found that a Dirichlet mode exists for all $b/d < 1$ if $n \leqslant 1$ and for $b/d = B(n)$ if $n \geqslant 1$ where $B(n)$ is monotone decreasing with $n$ and $B(1) = 1$, $B(\infty) = \frac{1}{2}$. Since for $n \leqslant 1$ all cylinders of this type of cross-section are contained within the triangular cross-section given by $n = 1$, it is tempting to surmise that a Dirichlet mode exists for *all* cross-sections contained within the open region bounded by $y = 0$, $|x|/a + |y|/d = 1$. This does not follow since it is not true that $I > 0$ for all even $f$ satisfying $f(x) < d(1 - x/a)$.

It is not yet clear how the methods of Evans *et al.* (1994) can be extended to cover the cases of multiple cylinders considered in this paper.

## 3. Results

In computing both the Neumann and Dirichlet trapped modes we need to find the real zeros of the determinant of the system (2.24) in the case of two equal cylinders, or, for a more general geometrical configuration, the real zeros of the determinant of the system (2.19). In the case of Neumann modes, we use (2.25)–(2.30) and for Dirichlet modes we use a slightly modified version of (2.25)–(2.30) (see §2.3).

In order to solve both systems (2.23) and (2.19) numerically, we first need to truncate the system to a size $M$, say, which is equivalent to discarding the Fourier modes $A^k_{M+1}, A^k_{M+2}, \ldots$ about each cylinder *a priori*. We therefore need to be careful in choosing $M$ to ensure that enough modes are taken to approximate the trapped mode solution to an acceptable degree of accuracy. In the case of a single cylinder, as described in Callan *et al.* (1991), as few modes as $M = 3$ or 4 is sufficient for five decimal places of accuracy provided $\mu(= a/d) \lesssim \frac{1}{2}$ and even for $\mu = 1$, only 12 modes are needed for a similar accuracy. In the case of multiple cylinders, the criterion for choosing $M$ is more complicated since one has to take into account the expected interaction effect of one cylinder on a neighbouring cylinder. Indeed in the results that follow we have allowed cylinders to touch and careful computational experiments suggest that for moderately sized cylinders $M = 24$ is good enough for less than 0.5% error at touching. However, it seems that a large number of modes is necessary for two cylinders almost spanning the width of the channel which is why the curves that follow in figure 3 stop some way short of $\mu = 1$. This is perhaps due to the gradual isolation of an interior fluid region from the rest of the channel with two cylinders approaching $\mu = 1$. Most of the results that follow are in terms of a cylinder separation parameter, $\lambda$, chosen to lie within the interval $\lambda \in [1, 6]$, where $\lambda = 1$ is always associated with touching cylinders. With this definition, we choose $M$ to be the integer part of $24/\lambda^{3/2} + 12\mu$ and expect results that are accurate to at least two decimal places. It remains for us to look for trapped mode frequencies by finding real zeros of the determinant of the truncated $2M \times 2M$ version of (2.24)

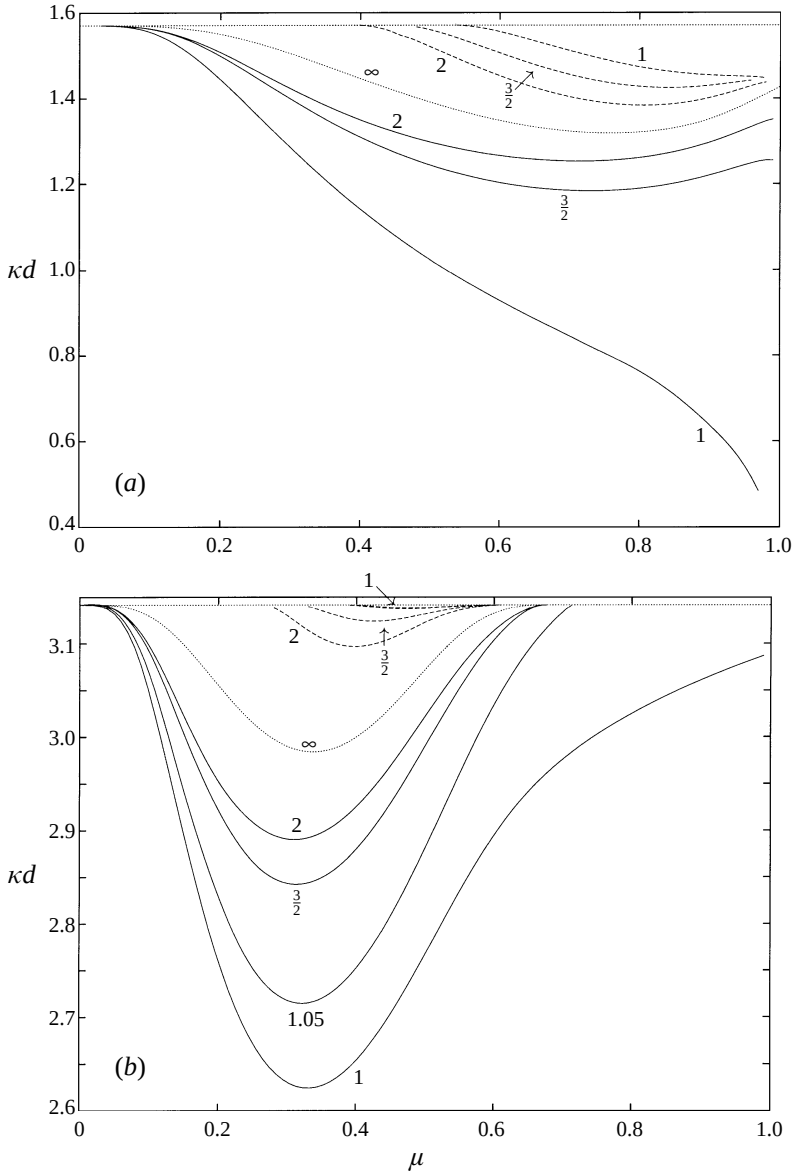


FIGURE 3. Variation of (*a*) Neumann and (*b*) Dirichlet trapped mode frequencies as $\mu$ varies in the case of two cylinders for different values of the spacing parameter $\lambda$ (shown against the curves). Symmetric modes (——), antisymmetric modes (— — —).

or the $NM \times NM$ version of (2.19). This is done using an LU decomposition routine to provide a value of the determinant which is used within a root-solving algorithm.

The number of possible configurations of cylinders we could consider is of course limitless but we shall concentrate mainly on the case of two identical cylinders because of its connection with *finite* double arrays of cylinders which occur in offshore floating structures as discussed in the Introduction. The non-dimensional trapped mode wavenumber $\kappa d$ is in this case a function of two dimensionless parameters $\mu$ and $\lambda$

describing the size and spacing of the centres of the cylinders. We choose $\mu = a/d$ and let the centres of the cylinders be located at $(\pm\lambda a, 0)$ so that $\lambda$ is a spacing parameter being the ratio of cylinder separation to cylinder diameter. When $\lambda = 1$ the cylinders are touching and as $\lambda \to \infty$ we would expect results for the trapped modes to approach the single-cylinder results as the interaction between them diminishes. In fact since the trapped modes are a localized phenomenon we might expect the single-cylinder results to be approached for relatively small values of $\lambda$. This proves to be the case as figure 3 illustrates. Here, Neumann and Dirichlet trapped mode wavenumbers $\kappa d$ obtained by computing the real zeros of the determinant in the system (2.24) are plotted against $\mu$ for different $\lambda$. Also shown is the unique curve for both the Neumann and Dirichlet trapped modes for an isolated cylinder which we label $\lambda = \infty$. We consider the Neumann modes first, all of whose wavenumbers satisfy $\kappa d < \pi/2$. The solid curves are symmetric Neumann trapped modes obtained by choosing $s = 1$ in equation (2.24) whilst the dashed curves above the $\lambda = \infty$ curve are all antisymmetric Neumann trapped modes and obtained by choosing $s = 0$ in equation (2.24). We can draw the following conclusions about the Neumann modes from figure 3. For sufficiently large $\mu$ there exist *two* trapped modes, a low frequency symmetric mode and a higher frequency antisymmetric mode, for each value of $\lambda$. However, for fixed $\lambda$, as $\mu$ decreases a value is reached at which the antisymmetric mode disappears. This may be compared with the case of a cylinder of rectangular cross-section in a channel considered by Evans & Linton (1991) where an additional trapped mode, alternately antisymmetric and symmetric, appears each time the dimension of the rectangular cylinder along the tank increases beyond an integer multiple of the channel width. We have re-computed the Neumann trapped modes and obtained new results for the Dirichlet trapped modes for the rectangular cylinder using an efficient and accurate Galerkin approximation similar to that used by Porter (1995) in a related problem. See also Evans & Fernyhough (1995). The corresponding results for a rectangle of sides $2a$, $4a$ which circumscribes the two circular cylinders when touching ($\lambda = 1$) give fairly close agreement with the Neumann modes in figure 3($a$) but not with the two Dirichlet modes in figure 3($b$), one of which persists for all $\mu \in (0, 1)$ whereas for the rectangle there is a cut-off at $\mu = \frac{1}{2}$.

It appears from figure 3 that, as expected, the curves for increasing $\lambda$ approach the single-cylinder results. This is more clearly seen in figure 4 which plots $\kappa d$ against $\lambda$ for $\mu = \frac{1}{2}$. Both the Dirichlet and the Neumann curves rapidly approach the corresponding single-cylinder trapped mode frequency as $\lambda$ increases. Notice how the antisymmetric Neumann mode cuts off below a certain value of $\lambda > 1$ whilst the antisymmetric Dirichlet mode persists down to touching at $\lambda = 1$. This behaviour can also be seen from figure 3 by considering the intersection of $\mu = \frac{1}{2}$ with curves of different $\lambda$. However it is also clear from figure 3 that in general the behaviour of the Dirichlet modes is more complicated than that of the Neumann modes. Maniar & Newman (1997) have shown that for an isolated cylinder Dirichlet modes only exist for $0 < \mu \lesssim 0.677$ and this is confirmed in figure 3 by the $\lambda = \infty$ curve where we find the improved estimate 0.6789 as the cut-off value. The presence of a second identical cylinder widens the range of $\mu$ for which (symmetric) Dirichlet modes exist and this range increases slowly as the gap between the cylinders is reduced. Thus, even for $\lambda = 1.05$ when the fluid gap is only 5% of a cylinder diameter, the range of existence has only increased up to $\mu \approx 0.772$. However, computations right down to $\lambda = 1$, corresponding to touching, suggest that a symmetric Dirichlet mode exists for *all* $\mu \in (0, 1)$. Note that at $\lambda = \mu = 1$ each of the two exterior fluid regions is the same as the region exterior to a single cylinder with $\mu = 1$ for which figure 3 shows there is no

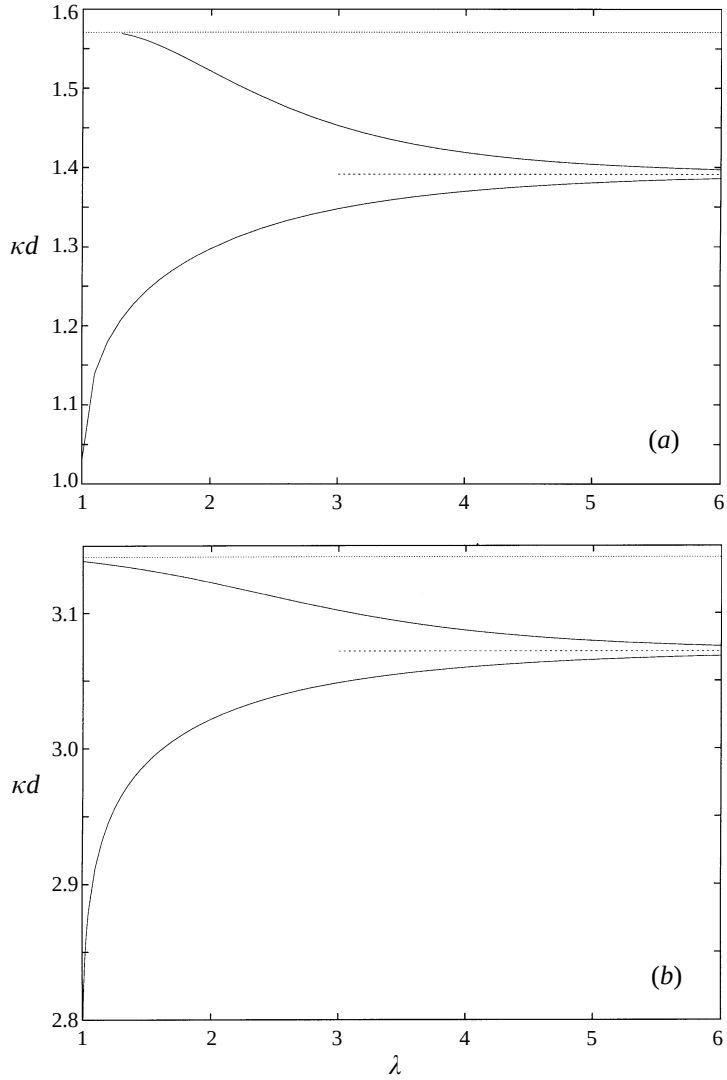


FIGURE 4. Variation of (*a*) Neumann and (*b*) Dirichlet trapped mode frequencies for two cylinders, both $\mu = \frac{1}{2}$ as the spacing parameter, $\lambda$, varies.

solution. One explanation is that in this limit the trapped mode frequency coincides with a sloshing frequency in the two identical bounded cusped interior regions. In addition to this complicated behaviour for $\lambda \approx 1$, the antisymmetric Dirichlet modes, just as for the Neumann modes, also manifest a cut-off below certain values of $\mu$ for each $\lambda$ so that the overall picture is one of existence of antisymmetric Dirichlet modes in intervals of $\mu$ for given $\lambda$ which increase in length with increasing $\lambda$ up to $0 < \mu \lesssim 0.6789$ and the existence of symmetric Dirichlet modes for all $\mu$ for $\lambda$ sufficiently close to unity, or a cut-off above some value $\mu_0$ with $0.6789 \lesssim \mu_0 \leqslant 1$ for each $\lambda$. This is illustrated in figure 5 which repeats figure 4 with $\mu = 0.8$. In this case the Neumann antisymmetric mode exists for all $\lambda \geqslant 1$, whilst for $\mu = 0.8$ the antisymmetric Dirichlet mode does not exist and the symmetric mode only cuts in for values of $\lambda$ close to touching.

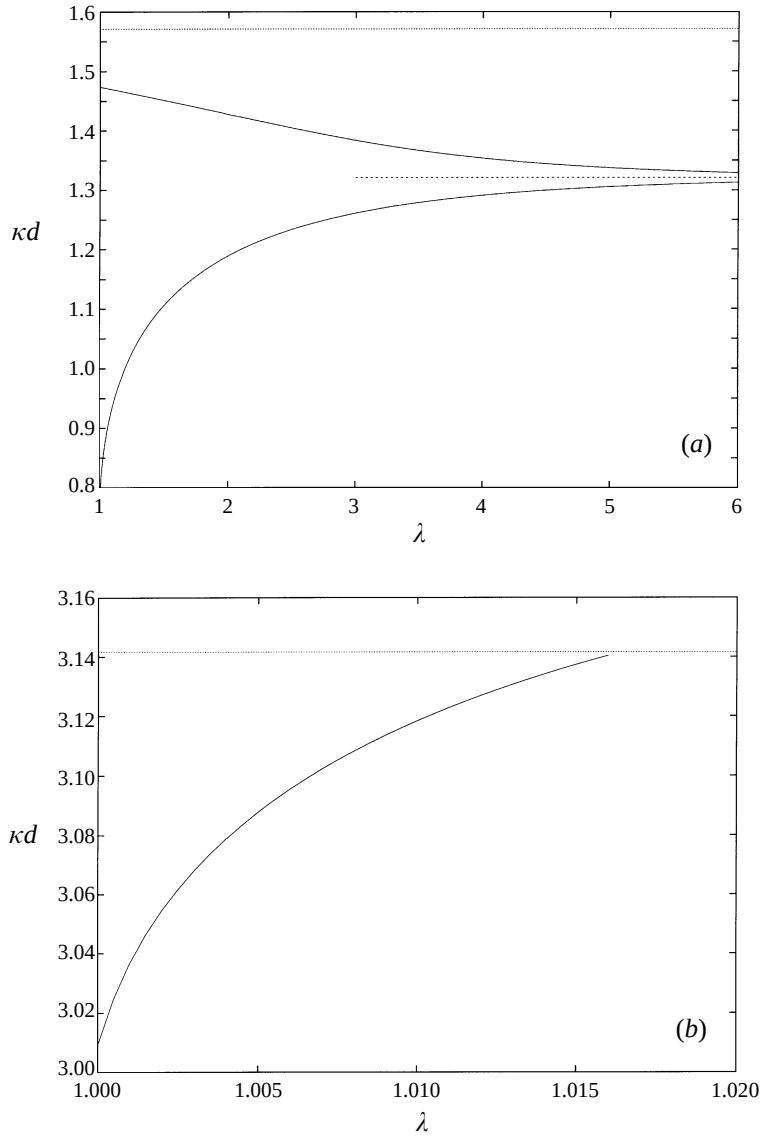


FIGURE 5. Variation of (*a*) Neumann and (*b*) Dirichlet trapped mode frequencies for two cylinders, both $\mu = \frac{4}{5}$ as the spacing parameter, $\lambda$, varies.

It is possible to remove the channel walls and regard both types of trapped modes as oscillations between adjacent pairs of cylinders in a doubly infinite row, the Neumann modes having an antinode at each mid-plane between pairs of cylinders and the Dirichlet modes a node. Following the discussion of Maniar & Newman (1997) that a *finite* single row containing many cylinders could experience large forces and free-surface motions at frequencies close to the Neumann and Dirichlet trapped modes for a single cylinder in a channel, or its equivalent *infinite* row of cylinders, we should expect that the peaks in figures 1(*a*) and 1(*b*) which give the maximum in-line exciting force on the middle pair of cylinders in a double row of $2 \times 9$ cylinders due to head seas to be close to the corresponding symmetric trapped modes. In figures

1(*a*),(*b*) the distance between two cylinders in a pair is 4*a* so that in both figures the corresponding doubly infinite row requires $\lambda = 2$. It is clear from figure 4 at $\lambda = 2$ that this is indeed the case. Thus the computed values of the symmetric Neumann and Dirichlet trapped mode wavenumbers for $\mu = \frac{1}{2}$ are $\kappa d = 1.29771$ and $\kappa d = 3.02157$ respectively compared to the peaks at 1.256 and 3.024 in figure 1(*a*) whilst for $\mu = \frac{1}{4}$ the trapped modes at $\kappa d = 1.46567$ and 2.90894 compare to the peaks at 1.400 and 2.856 respectively in figure 1(*b*). The other peaks in figure 1(*a*, *b*) are believed to correspond to nearly trapped waves. Notice how the dominant mode in figure 1(*a*) when $\mu = \frac{1}{2}$ is a symmetric Neumann mode whereas in figure 1(*b*) when $\mu = \frac{1}{4}$ the symmetric Dirichlet mode dominates. The same behaviour was found by Maniar & Newman (1997, figure 1) in considering a single row of cylinders.

Because figure 1 describes the exciting forces in head seas, it shows no evidence of the antisymmetric Neumann trapped modes at $\mu = \frac{1}{2}$ shown in figure 4 for $\lambda = 2$. Computations for a double row of nine cylinders in obliquely incident waves having an antisymmetric component again provide little indication of the antisymmetric mode whilst the peak for the symmetric mode is reduced. It appears to be difficult to generate a significant peak close to the antisymmetric trapped modes in a finite double row by using a physically realistic wave train. However it proves possible using equal and opposite obliquely incident waves which are antisymmetric about the mid-line between the two rows of cylinders to create a similar amplification to that shown in figure 1 in the wave forces on the middle cylinders close to the antisymmetric Neumann mode for $\mu = \frac{1}{2}$.

We now consider two unequal cylinders with $\mu = 0.3$ and 0.7 and centres at $(-0.3\lambda d, 0)$ and $(0.7\lambda d, 0)$ so that again $\lambda = 1$ is touching. There is no longer symmetry and the full equations (2.19) must be used. It can be seen from figure 6 that the two Neumann modes, which exist for all $\lambda$, tend to the appropriate values for isolated cylinders of these radii as $\lambda$ increases. From figure 3 it is clear that the higher frequency curve approaches the value for the 0.3 radius cylinder and the lower curve approaches the 0.7 radius cylinder and we may infer from this that the eigenmodes corresponding to points on the upper (lower) curve are larger (smaller) in the vicinity of the smaller cylinder. We shall return to this later. Since from figure 3 there is no Dirichlet mode for an isolated cylinder with $\mu = 0.7$, we only expect to see a single curve for $\lambda$ large, corresponding to an isolated cylinder with $\mu = 0.3$. However there is no evidence of a further mode cutting in even for $\lambda \approx 1$ as would be the case for two identical cylinders with $\mu = 0.7$.

We can extend this to three different cylinders having radii $\mu = 0.8$, 0.2 and 0.5 and centres at the points $(-\lambda d, 0)$, $(0, 0)$ and $(0.7\lambda d, 0)$ respectively so that $\lambda = 1$ again refers to all three cylinders touching. The results are shown in figure 7 as the relative spacing increases with $\lambda$. It can be seen that as $\lambda$ increases there are three curves each approaching the corresponding isolated-cylinder result. The upper curve tending to the cylinder of radius 0.2 cuts out below a certain value of $\lambda$ leaving the remaining curves for all $\lambda$ down to touching. This is consistent with the results for a cylinder of rectangular cross-section and of dimensions 3*d* along the channel. There are only two curves for the Dirichlet case consistent with the absence of such a mode for an isolated cylinder with $\mu = 0.8$, but both curves persist for all $\lambda \geqslant 1$.

The occurrence of arrays of identical equally spaced cylinders in industrial applications beyond the offshore industry prompts us to return to this case to attempt a general understanding of what is happening. Thus figure 8 presents curves for four such cylinders each with $\mu = \frac{1}{2}$ from which we shall attempt to infer the behaviour

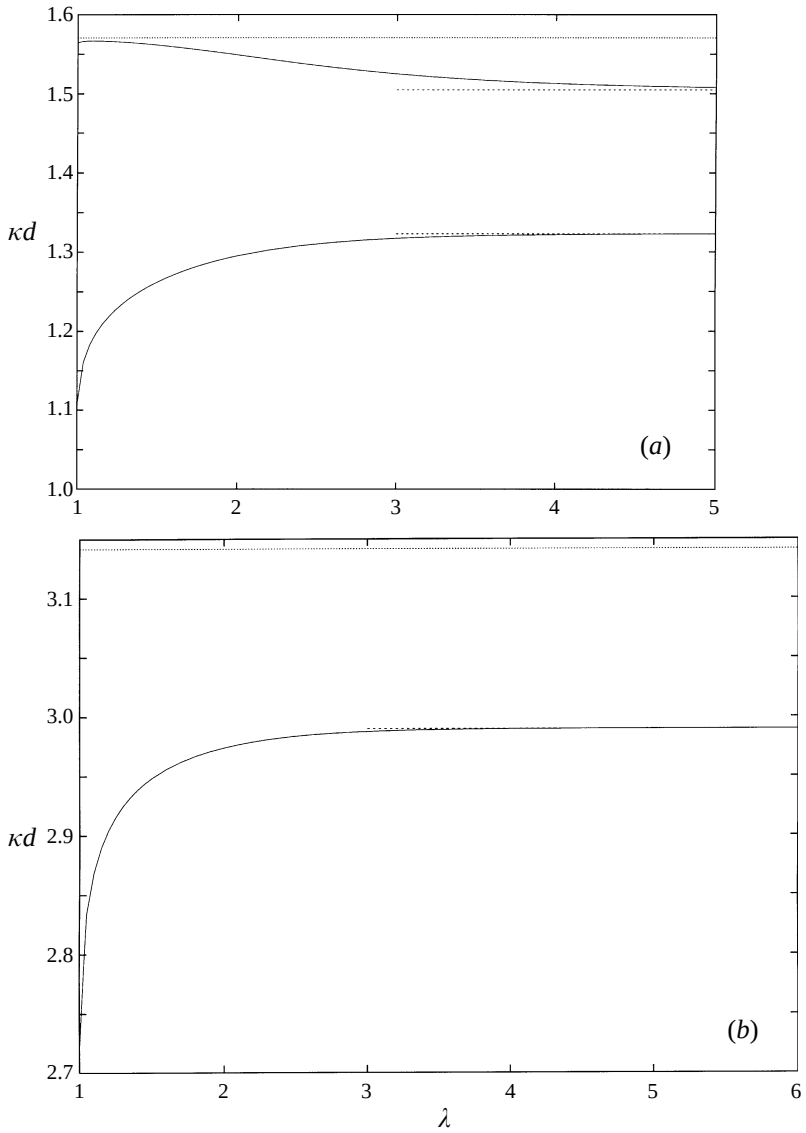


FIGURE 6. Variation of (*a*) Neumann and (*b*) Dirichlet trapped mode frequencies for two cylinders, $a_1/d = 0.3$, $a_2/d = 0.7$, as the spacing parameter, $\lambda$, varies.

in the general case of $N$ cylinders. It should be emphasized that the computing time required becomes large even for $N$ as low as 4. It is clear from figure 8 that for $N$ cylinders there will be $N$ Neumann modes for sufficiently large $\lambda$ each approaching the unique limit for a single cylinder at that value of $\mu$. As $\lambda$ reduces, some (or none) of the $N$ curves cut out, depending on the value of $\mu$, leaving $\leqslant N$ curves for $\lambda = 1$. The $N$ curves describe alternately symmetric and antisymmetric modes with respect to a vertical plane through the mid-point of the array perpendicular to the channel walls. The same qualitative behaviour appears to occur for Dirichlet modes provided (as in the case in figure 9 where $\mu = \frac{1}{2}$) there exists a Dirichlet mode at that value of $\mu$ for an isolated cylinder. If this is not the case, the situation is the same as

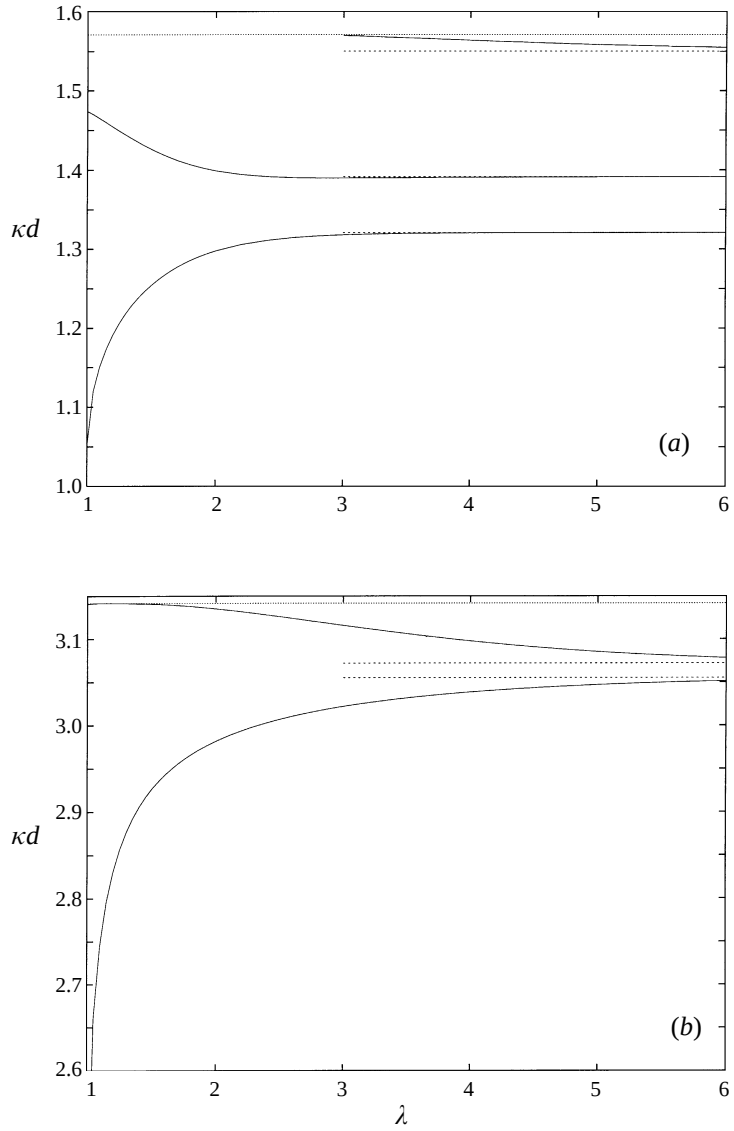


FIGURE 7. Variation of (*a*) Neumann and (*b*) Dirichlet trapped mode frequencies for three cylinders, $a_1/d = 0.8$, $a_2/d = 0.2$ and $a_3/d = 0.5$, as the spacing parameter, $\lambda$, varies.

described by figure 5 for the Dirichlet modes with only a single curve existing for a limited range of $\lambda$ close to touching, for any number of cylinders. As a final example using identical cylinders we consider the case of three cylinders, each having $\mu = \frac{1}{2}$ positioned at $(-4a, 0)$, $(0, 0)$ and $(2a\lambda, 0)$ so that two are touching when $\lambda = 1$. Figure 9 shows the variation in both types of trapped mode curves as the outer touching cylinder moves off with increasing $\lambda$ leaving the other two a distance $4a$ apart. For both Neumann and Dirichlet modes, for large $\lambda$ the middle curve approaches the value for an isolated cylinder whilst the two outer curves approach the symmetric and antisymmetric values given by $\lambda = 2$, $\mu = \frac{1}{2}$ in figure 3. As $\lambda$ decreases the

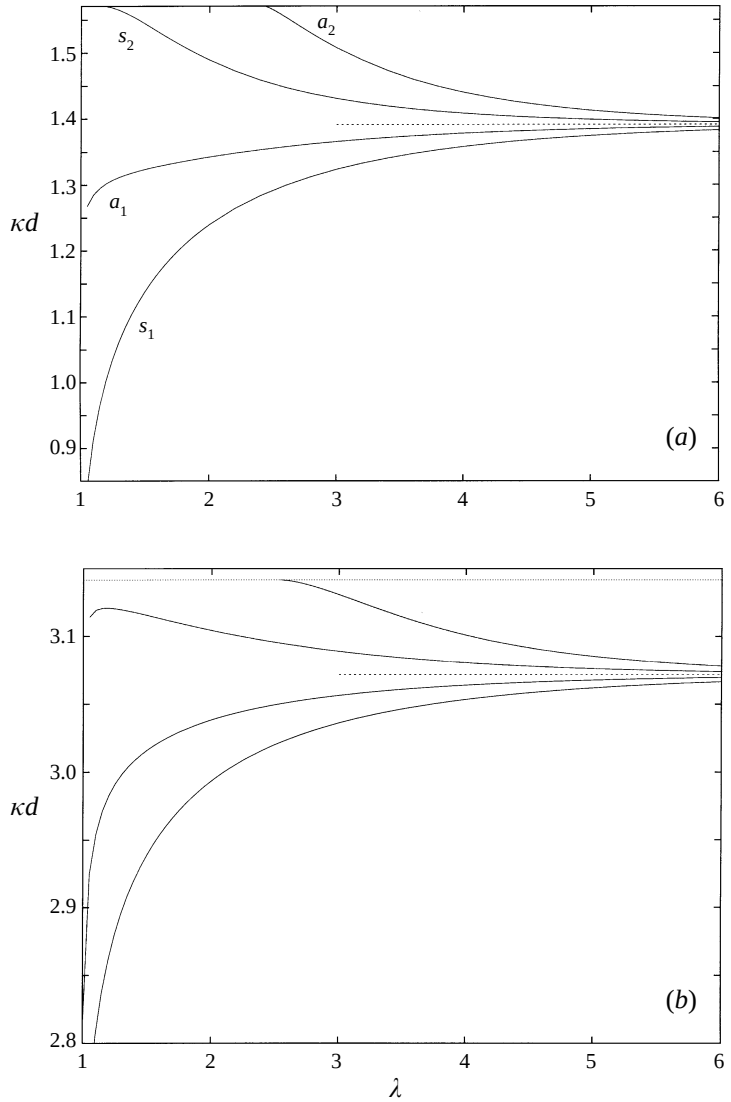


FIGURE 8. Variation of (*a*) Neumann and (*b*) Dirichlet trapped mode frequencies for four equal cylinders, $\mu = \frac{1}{2}$, evenly spaced, as the spacing parameter, $\lambda$, varies.

upper curve cuts out in each case leaving two curves of trapped modes down to touching.

### 3.1. *Relative wave amplitudes of trapped modes*

Each point on all the curves we have computed corresponds to a trapped mode and we can go back to the infinite systems of equations and determine a corresponding wave field. In the case of two identical cylinders, the motion near to one is either exactly in or out of phase with the motion near to the other. For all other configurations of cylinders this is not the case although for $N$ identical equally spaced cylinders this statement is true for the *overall* wave fields either side of a vertical plane perpendicular to the channel walls which divides the array equally. It is therefore of interest to examine the relative amplitudes of these trapped modes in one or two

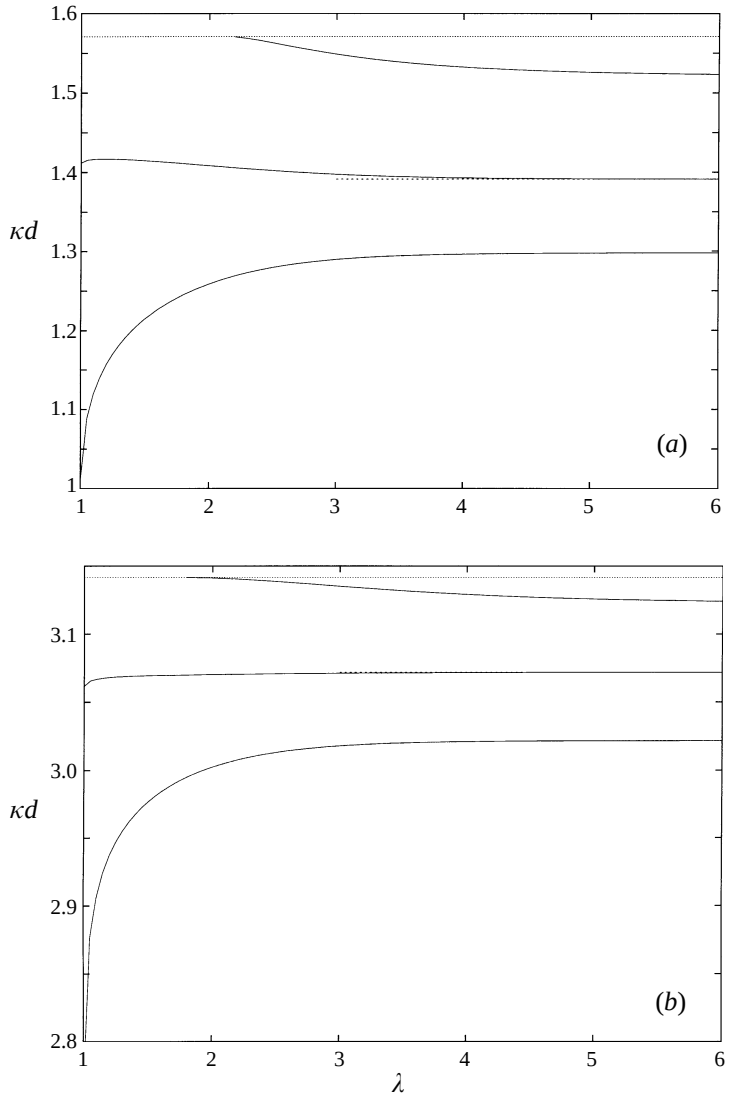


FIGURE 9. Variation of (*a*) Neumann and (*b*) Dirichlet trapped mode frequencies for three equal cylinders, $\mu = \frac{1}{2}$, when two are fixed and the third moves vs. the spacing parameter, $\lambda$.

cases. To do this we need an expression for the potential on cylinder $k$. This is obtained from (2.20) by putting $r_k = a_k$ and simplifying using a Wronskian for Bessel functions to give

$$\phi(a_k, \theta_k) = -\sum_{m=1}^{\infty} \frac{2A_m^k \sin m\theta_k}{\pi \kappa a_k J_m'(\kappa a_k)}. \tag{3.1}$$

There is no difficulty with the denominator since from (2.19), $A_m^k$ is zero whenever $J_m'(\kappa a_k)$ is so their ratio is well-defined. The $A_m^k$ are determined from (2.19) at the particular trapped mode as an eigenvector of the homogeneous system. This can easily be made a by-product of the trapped mode frequency computation which uses an LU decomposition method to determine the value of the determinant within a

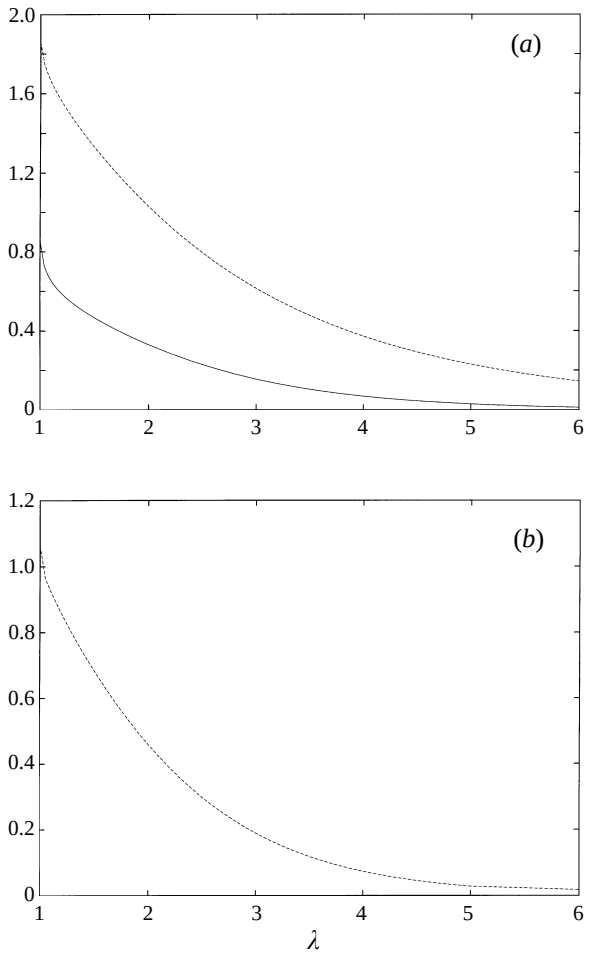


FIGURE 10. Relative maximum amplitudes of (*a*) the Neumann and (*b*) Dirichlet trapped mode oscillation about two cylinders radius 0.3 and 0.7 as the spacing parameter, $\lambda$, varies: ——, Amp(0.3)/Amp(0.7) corresponding to the lower curve in figure 6; - - -, is Amp(0.7)/Amp(0.3) corresponding to the upper curve in figure 6.

root-solving algorithm. Once the trapped mode frequency has been calculated to within a desired tolerance, a straightforward back substitution procedure involving the factor U only yields the coefficients $A_m^k$ scaled by $A_M^N$. Equation (3.1) is then used to compute

$$\mathrm{Amp}(a_k/d) = \max_{\theta_k \in (0,\pi)} \{|\phi(a_k, \theta_k)|\} \tag{3.2}$$

and $\mathrm{Amp}(a_k/d)/\mathrm{Amp}(a_j/d)$ determines the ratio of the maximum wave elevation at the cylinder of radius $a_k$ to that at the cylinder of radius $a_j$ at that trapped mode frequency.

We illustrate this by returning to the case of two unequal cylinders $k = 1, 2$ with $\mu = 0.3$ and 0.7 respectively shown in figure 6. In figure 10(*a*) the lower curve shows the variation of Amp(0.3)/Amp(0.7) with spacing along the *lower* Neumann curve in figure 6 which approaches the trapped mode wavenumber for a cylinder of radius 0.7 as $\lambda$ increases. Throughout the range of $\lambda$ the maximum amplitude is greater at

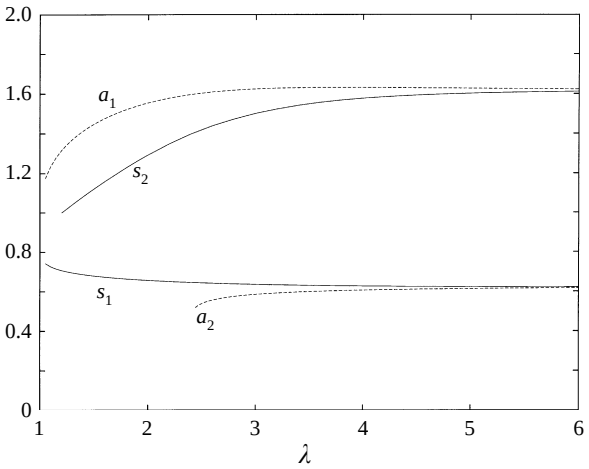


FIGURE 11. Relative maximum amplitudes of the Neumann trapped mode oscillation about cylinders 1 and 2 in an equally spaced array of four cylinders radius $\mu = \frac{1}{2}$ as $\lambda$ varies. The curves show $\mathrm{Amp}^{(1)}(\frac{1}{2})/\mathrm{Amp}^{(2)}(\frac{1}{2})$ corresponding to the four curves in figure 8(*a*).

the 0.7 cylinder than the 0.3 cylinder, the effect increasing as $\lambda$ increases and as the isolated-cylinder trapped mode value is approached. The upper curve describes the variation of Amp(0.7)/Amp(0.3) along the upper Neumann curve in figure 6 which approaches the trapped mode wavenumber for a cylinder of radius 0.3 as $\lambda$ increases. The shape of the curve is the same with the motion being dominated increasingly by the 0.3 radius cylinder as $\lambda$ increases, as expected. However for $\lambda \lesssim 2$ the motion near the 0.7 cylinder dominates, increasingly so down to touching. It would appear that the size of the cylinder compensates for being closer to the trapped mode wavenumber of the smaller cylinder. Turning now to the Dirichlet modes, there is only a single curve which approaches the isolated 0.3 radius cylinder. Thus in figure 10(*b*) the curve describes the variation Amp(0.7)/Amp(0.3) with $\lambda$ and again the motion is increasingly dominated by the motion near the 0.3 radius cylinder as $\lambda$ increases, as expected.

As a second example we consider the relative amplitudes in the case of four identical equally spaced cylinders with $\mu = \frac{1}{2}$, whose variation of trapped mode frequencies with $\lambda$ has already been presented in figure 8. We shall only discuss the Neumann case since similar behaviour occurs for the Dirichlet modes as shown in figure 8. Because of the symmetry we consider only the first two cylinders in the row, cylinders 3 and 4 having either equal or opposite amplitudes to cylinders 2 and 1 respectively depending on whether the trapped mode is symmetric or antisymmetric. We label the four curves in figure 8(*a*) starting with the lowest as $s_1$, $a_1$, $s_2$, $a_2$ ($s_1$ is the first symmetric mode, $a_1$ the first antisymmetric and so on). Figure 11 describes the variation of $\mathrm{Amp}^{(1)}(\frac{1}{2})/\mathrm{Amp}^{(2)}(\frac{1}{2})$ (the ratio of maximum amplitudes at cylinder 1 to cylinder 2) along each curve in figure 8. The surprising feature of the curves is their behaviour for large $\lambda$ when the trapped modes in figure 8 all approach the isolated trapped mode value. Thus the curves $a_1$ and $s_2$ appear to converge to a common value such that the maximum around the end cylinder is $\approx 1.6$ times that of its neighbour, whilst the curves $s_1$ and $a_2$ converge to a different lower value which in fact turns out to mean that the maximum motion around cylinder 2 is again $\approx 1.6$ times that around the end cylinder. It might have been expected that all four cylinders

would have converged to unity as $\lambda$ increased but the limit $\lambda = \infty$ would decouple the system (2.19) and the $A_m^k$ ($k = 1, 2, 3, 4$) would become independent. For any finite $\lambda$ the coupling remains, however weak, resulting in an apparent non-uniform limit for $\mathrm{Amp}^{(1)}(\frac{1}{2})/\mathrm{Amp}^{(2)}(\frac{1}{2})$ as $\lambda \to \infty$.

Because of the weak interaction between the adjacent cylinders it might be expected that a 'wide-spacing' approximation utilizing the trapped mode properties of each cylinder in isolation could be used. However such approximation succeeds by transferring information between cylinders through planes with the neglect of the local field. Since in a trapped mode problem there is no radiated wave and only a local field, such an approach will not work.

## 4. Conclusion

A combination of multipole expansions methods and the use of addition theorems for Bessel functions has enabled accurate computations to be made of the trapped modes which arise in a narrow wave channel containing any number of bottom-mounted circular cylinders of arbitrary size and spacing positioned on the centreplane of the channel. It has been shown that in general there are up to $N$ trapped mode frequencies below the lowest cut-off for the channel, corresponding to any configuration of $N$ cylinders, the precise number depending critically on whether the mode is of Dirichlet or Neumann type and on the precise geometry of the configuration. As has been pointed out by Maniar & Newman (1997) trapped modes of both types are important in offshore engineering where long floating structures such as bridges or floating airports requiring many cylindrical supports are being considered, since large forces at frequencies close to the trapped mode frequencies can occur on those supports near the centre of a long periodic array.

The present paper, as well as extending our fundamental understanding of trapped modes in channels, has applications in other areas and in particular in acoustics where they are termed acoustic resonances. Our extension to any number of cylinders suggests that in any situation where multiple periodic arrays of cylinders occur, such as banks of heat exchangers for example, large forces can occur if the frequency of the acoustical excitation should coincide with the trapped mode frequencies. These implications are currently being explored.

R.P. is supported by EPSRC research grant no. GR/K67526.

*Note added in proof.* Whilst this paper was being prepared for publication one of the authors (R.P.) discovered, numerically, further Neumann modes for multiple cylinders for $\mu(= a/d)$ sufficiently large. For a single cylinder, the new mode, in addition to being antisymmetric with respect to the centreplane of the channel, is also antisymmetric about a plane through the centre of the cylinder which is perpendicular to the channel walls. For two identical cylinders the new modes approach the corresponding value for a single cylinder as the spacing increases. The only figure affected is figure 3 which is now completed by the inclusion of the sequence of curves shown in figure 12.

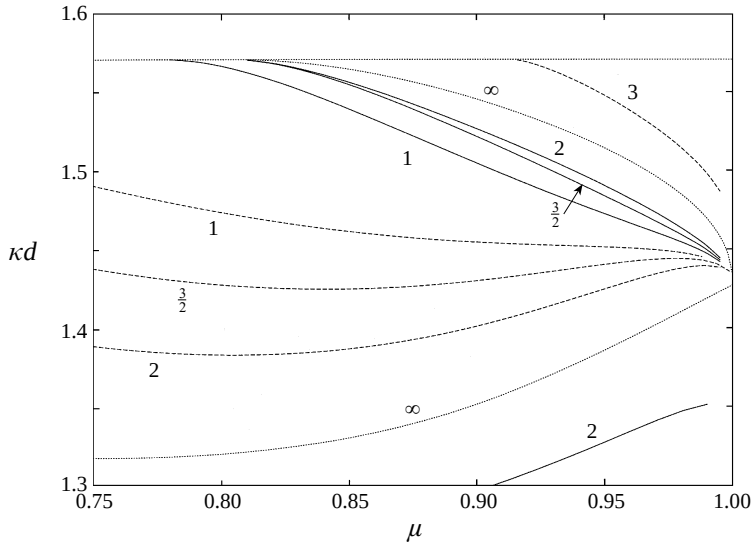


FIGURE 12. Part of figure 3: Variation of Neumann trapped mode frequencies as $\mu$ varies in the case of two cylinders for different values of the spacing parameter $\lambda$ (shown against the curves). Symmetric modes (——), antisymmetric modes (– – –). Single cylinder trapped modes (..... and labellled by $\infty$).

## Appendix A. Multipole derivation

We start with the following integral representation of the Hankel function, see Callan *et al.* (1991, Appendix A):

$$H_n(\kappa r)\mathrm{i}^n\mathrm{e}^{\mathrm{i}n\theta} = -\frac{\mathrm{i}}{\pi}\int_{-\infty}^{\mathrm{i}\pi+\infty} \mathrm{e}^{\mathrm{i}\kappa x\cosh v}\mathrm{e}^{\kappa y\sinh v}\mathrm{e}^{nv}\,\mathrm{d}v, \qquad 0\leqslant\theta\leqslant\pi \tag{A 1}$$

where $x = r\cos\theta$, $y = r\sin\theta$. It follows that

$$\begin{aligned} H_n(\kappa r)\sin n\theta &= \frac{(-\mathrm{i})^n}{2\pi}\int_{-\infty}^{\mathrm{i}\pi+\infty} \mathrm{e}^{\gamma y-nv}\{\mathrm{e}^{\mathrm{i}\kappa x\cosh v} - (-1)^n\mathrm{e}^{-\mathrm{i}\kappa x\cosh v}\}\,\mathrm{d}v \\ &= \frac{\mathrm{i}}{\pi}\int_{-\infty}^{\mathrm{i}\pi+\infty} \mathrm{e}^{\gamma y-nv}\sin(\kappa x\cosh v - n\pi/2)\,\mathrm{d}v, \qquad 0\leqslant\theta\leqslant\pi \end{aligned} \tag{A 2}$$

where $\gamma = \kappa\sinh v$. This vanishes on $\theta = 0$. We need to add an expression to the integral (A 2) which is odd in $y$ such that the combination also satisfies zero normal derivative on $y = d$. Thus, we note that

$$\frac{\partial}{\partial y}\{\mathrm{e}^{\gamma y} + A(v)\sinh\gamma y\} = 0 \tag{A 3}$$

on $y = d$ when

$$A(v) = -\mathrm{e}^{\gamma d}/\cosh\gamma d. \tag{A 4}$$

So we define our multipoles by

$$\psi_n(r,\theta) = H_n(\kappa r)\sin n\theta - \frac{\mathrm{i}}{\pi}\int_{-\infty}^{\mathrm{i}\pi+\infty} \frac{\mathrm{e}^{\gamma d-nv}\sinh\gamma y}{\cosh\gamma d}\sin(\kappa x\cosh v - n\pi/2)\,\mathrm{d}v \tag{A 5}$$

$$= \frac{\mathrm{i}}{\pi}\int_{-\infty}^{\mathrm{i}\pi+\infty} \frac{\cosh\gamma(y-d)}{\cosh\gamma d}\mathrm{e}^{-nv}\sin(\kappa x\cosh v - n\pi/2)\,\mathrm{d}v. \tag{A 6}$$

The form of (A 5) clearly satisfies $\psi_n(r,0)=0$, whilst the form of (A 6) shows that $\partial\psi_n/\partial y=0$ on $y=d$.

The contour in the integral in (A 6) is split into three parts: $C_1=(-\infty,0)$, $C_2=(0,\mathrm{i}\pi)$, $C_3=(\mathrm{i}\pi,\mathrm{i}\pi+\infty)$. Then straightforward changes of variable applied to (A 6) with $n$ even and odd considered separately give the following result:

$$\psi_{2n}(r,\theta)=\frac{2\mathrm{i}(-1)^n}{\pi}\int_0^\infty\frac{\cosh\gamma(y-d)}{\cosh\gamma d}\sinh 2nv\sin(\kappa x\cosh v)\,\mathrm{d}v$$
$$-\frac{2\mathrm{i}}{\pi}\int_0^{\pi/2}\frac{\cos\beta(y-d)}{\cos\beta d}\sin(\kappa x\sin u)\sin 2nu\,\mathrm{d}u \tag{A 7}$$

and

$$\psi_{2n+1}(r,\theta)=\frac{-2\mathrm{i}(-1)^n}{\pi}\int_0^\infty\frac{\cosh\gamma(y-d)}{\cosh\gamma d}\sinh(2n+1)v\cos(\kappa x\cosh v)\,\mathrm{d}v$$
$$+\frac{2\mathrm{i}}{\pi}\int_0^{\pi/2}\frac{\cos\beta(y-d)}{\cos\beta d}\cos(\kappa x\sin u)\cos(2n+1)u\,\mathrm{d}u \tag{A 8}$$

where $\beta=\kappa\sin u$. The expression (A 8) agrees with Callan *et al.* (1991, Appendix A). Since neither $\cosh\gamma d$ nor $\cos\beta d$ vanishes on the paths of integration, provided $\kappa d<\pi/2$, it follows from the Riemann–Lebesgue lemma that $\psi_n(r,\theta)\to 0$ as $|x|\to\infty$. Clearly, from (A 7), (A 8), $\psi_n(r,\theta)$ is pure imaginary, and so from (A 5) discarding a factor i, we define

$$\psi_n(r,\theta)=Y_n(\kappa r)\sin n\theta-\mathrm{Re}\frac{1}{\pi}\int_{-\infty}^{\mathrm{i}\pi+\mathrm{i}\infty}\frac{\mathrm{e}^{\gamma d-nv}\sinh\gamma y}{\cosh\gamma d}\sin(\kappa x\cosh v-n\pi/2)\,\mathrm{d}v. \tag{A 9}$$

In the case of Dirichlet modes, instead of satisfying (A 3), we impose $\mathrm{e}^{\gamma y}+A(v)\sinh\gamma y=0$ on $y=d$ giving

$$A(v)=-\mathrm{e}^{\gamma d}/\sinh\gamma d. \tag{A 10}$$

Then following the procedure outlined above shows that the Dirichlet multipoles are indeed purely imaginary for $\kappa d<\pi$ and are thus given by

$$\psi_n(r,\theta)=Y_n(\kappa r)\sin n\theta-\mathrm{Re}\frac{1}{\pi}\int_{-\infty}^{\mathrm{i}\pi+\mathrm{i}\infty}\frac{\mathrm{e}^{\gamma d-nv}\sinh\gamma y}{\sinh\gamma d}\sin(\kappa x\cosh v-n\pi/2)\,\mathrm{d}v. \tag{A 11}$$

The only change has been in the replacement of $\cosh\gamma d$ by $\sinh\gamma d$ in the denominator of the integrand.

## Appendix B. Coordinate shifts

We are required to transfer $Y_n(\kappa r_j)\sin n\theta_j$ where $(r_j,\theta_j)$ are measured from $(d_j,0)$ to coordinates $(r_k,\theta_k)$ associated with the cylinder placed at $(d_k,0)$ and vice versa. We use Graf's Addition theorem for Bessel functions (Watson 1966) applied to the triangle with sides of length $r_j$, $r_k$, $|d_k-d_j|$ in figure 2 and consider the cases of $d_j<d_k$, $d_j>d_k$ separately.

The result is

$$Y_n(r_j)\sin n\theta_j=\sum_{m=1}^{\infty}F_{mn}^{jk}J_m(\kappa r_k)\sin m\theta_k \tag{B 1}$$

where

$$F_{mn}^{jk}=Y_{n-m}(\kappa|d_k-d_j|)\cos(n-m)\gamma_{jk}-(-1)^mY_{n+m}(\kappa|d_k-d_j|)\cos(n+m)\gamma_{jk} \tag{B 2}$$

with

$$\gamma_{jk} = \begin{cases} 0, & d_j < d_k \\ \pi, & d_j > d_k. \end{cases} \tag{B 3}$$

Notice that

$$F^{jk}_{mn} = (-1)^{n-m} F^{kj}_{mn} = (-1)^{n-m} F^{jk}_{nm}. \tag{B 4}$$

The shift in coordinates for the integrand in (2.10) uses the following result:

$$\mathrm{e}^{\mathrm{i}\kappa x_j \cosh v} \sinh \gamma y_j = -2\mathrm{i} \sum_{m=1}^{\infty} \mathrm{e}^{\mathrm{i}m\pi/2} J_m(\kappa r_j) \sin m\theta_j \sinh mv, \qquad j = 1, \ldots, N \tag{B 5}$$

which is derived from the identity (Watson 1966, p.15)

$$\exp\{\tfrac{1}{2} z(\tau - \tau^{-1})\} = J_0(z) + \sum_{n=1}^{\infty} (\tau^n + (-1)^n \tau^{-n}) J_n(z) \tag{B 6}$$

with the substitutions $z = \kappa r_j$, $\tau = \mathrm{i}\mathrm{e}^{\pm \mathrm{i}\theta_j} \mathrm{e}^{v}$. Using $x_j = d_k - d_j + x_k$ and $y_j = y_k$ in (B 5) gives

$$\mathrm{e}^{\mathrm{i}\kappa x_j \cosh v} \mathrm{e}^{-\mathrm{i}n\pi/2} \sinh \gamma y_j = -2\mathrm{i} \mathrm{e}^{\mathrm{i}\kappa(d_k - d_j)\cosh v} \sum_{m=1}^{\infty} \mathrm{e}^{\mathrm{i}(m-n)\pi/2} J_m(\kappa r_k) \sin m\theta_k \sinh mv \tag{B 7}$$

and taking the imaginary part leaves us with

$$\sinh \gamma y_j \sin(\kappa x \cosh y_j - n\pi/2)$$
$$= -2 \sum_{m=1}^{\infty} \cos\{\kappa(d_k - d_j)\cosh v + \tfrac{1}{2}(m-n)\pi\} J_m(\kappa r_k) \sin m\theta_k \sinh mv. \tag{B 8}$$

## REFERENCES


Callan, M., Linton, C. M. & Evans, D. V. 1991 Trapped modes in two-dimensional waveguides. *J. Fluid Mech.* **229**, 51–64.

Davies, E. B. & Parnovski, L. 1997 Trapped modes in acoustic waveguides. *Q. J. Mech. Appl. Maths* (submitted).

Evans, D. V. & Fernyhough, M. 1995 Edge waves along periodic coastlines. Part 2. *J. Fluid Mech.* **46**, 644–656.

Evans, D. V., Levitin, M. & Vassiliev, D. 1994 Existence theorems for trapped modes. *J. Fluid Mech.* **261**, 21–31.

Evans, D. V. & Linton, C. M. 1991 Trapped modes in open channels. *J. Fluid Mech.* **225**, 153–175.

Evans, D. V. & Linton, C. M. 1994 Acoustic resonance in ducts. *J. Sound Vib.* **173**, 85–94.

Evans, D. V. & Porter, R. 1997 Trapped modes embedded in the continuous spectrum. *Q. J. Mech. Appl. Maths* (submitted).

Linton, C. M. & Evans, D. V. 1990 The interaction of waves with arrays of vertical circular cylinders. *J. Fluid Mech.* **215**, 549–569.

Linton, C. M. & Evans, D. V. 1992 Integral equations for a class of problems concerning obstacles in waveguides. *J. Fluid Mech.* **245**, 349–365.

Linton, C. M. & McIver, P. 1996 The scattering of water waves by an array of circular cylinders in a channel. *J. Eng. Maths.* **30** 661–682.

Maniar, H. D. & Newman, J. N. 1997 Wave diffraction by a long array of cylinders. *J. Fluid Mech.* **339**, 309–330.

McIver, M. & Linton, C. M. 1995 On the non-existence or otherwise of trapped modes in acoustic waveguides. *Q. J. Mech. Appl. Maths* **43**, 543–555.

PARKER, R. & STONEMAN, S. A. T. 1989 The excitation and consequencies of acoustic resonances in enclosed fluid flow around solid bodies. *Proc. Inst. Mech. Engrs.* **203**, 9–19.

PORTER, R. 1995 Complementary methods and bounds in linear water waves. PhD Thesis, University of Bristol.

WATSON, G. N. 1966 *A Treatise on the Theory of Bessel Functions*, 2nd edn. Cambridge University Press.